

## 1.2 Ignition by Capacitance Sparks and Non-Thermal Plasmas

---

Johann-Robert Kummer, Stefan Essmann, Detlev Markus,  
Holger Grosshans, Ulrich Maas

### Abstract

For optimization of combustion engines understanding the ignition of combustible mixtures by electrical discharges is of crucial importance. A combined experimental-numerical approach is employed to gain deeper insight into the related physicochemical processes during the ignition by thermal and non-thermal plasmas. In both applications energies near the minimum energy necessary for ignition have been imposed. The temporal development of the plasma kernel and the shock wave measured using a schlieren method in combination with numerical simulations were used to quantify the ignition efficiency of a capacitance sparks. Radial profiles of OH radicals measured by laser induced fluorescence (LIF) were compared with numerical results to validate the numerical tools which now can be used to model ignition of advanced biofuels. Volumetric ignition by non-thermal plasmas has been investigated through numerical simulations which were used to examine the temporal development of temperature and radicals inside the plasma channel in detail.

### Kurzfassung

Für die Optimierung von Verbrennungsmotoren ist das Verständnis der Zündung von brennbaren Gemischen durch elektrische Entladungen von entscheidender Bedeutung. Ein kombinierter experimentell-numerischer Ansatz wird verwendet, um tiefere Einblicke in die physikalisch-chemischen Prozesse während der Zündung durch thermische und nicht-thermische Plasmen zu erhalten. Bei beiden Anwendungsbeispielen wurden Energien im Bereich der mindestens zur Zündung notwendigen Energie untersucht. Die zeitliche Entwicklung des Plasmakerns und der Stoßwelle mittels einer Schlieren-Methode zusammen mit numerischen Simulationen wurde verwendet, um die Effizienz einer Funkenzündung zu quantifizieren. Radiale Profile von OH-Radikalen, die durch laserinduzierte Fluoreszenz (LIF) gemessen wurden, werden mit numerischen Ergebnissen verglichen, um die numerischen Werkzeuge zu validieren, die nun zur Modellierung der Zündung nachhaltig erzeugter Biokraftstoffe verwendet werden können. Eine volumetrische Zündung kann mit nichtthermischen Plasmen erreicht werden. Hier wurden numerische Simulationen verwendet, um die zeitliche Entwicklung von Temperatur und Radikalen im Plasmakanal im Detail zu untersuchen.

## 1 Introduction

The need for clean combustion engines has grown in scope and importance over the years due to increasing shortage of energy resources and growing future environmental concerns. The transportation sector of the developed world depends mainly on energy released during the burning of fossil fuels, such as coal, oil, and natural gas. However, the release of greenhouse gases contributes to global climate change. In 2014, transport was responsible for 20 % of the direct CO<sub>2</sub> emissions in Germany [1], mainly due to road traffic. To meet transport demands of the future, there is a need to find alternative energy sources and alternative combustion engines especially with respect to the growing need for energy from the emerging countries. The EU's renewable energy directive 2009/28/EC demands a reduction of greenhouse gas emissions by at least 20 % and an increase of the share of renewable energy to at least 20 % of consumption by 2020 [2]. All EU countries are also required to have at least a 10 % share of renewable energy in their transportation sector. It can be expected that the EU will increase its climate, renewable energy and energy savings targets in order to achieve the Paris climate conference (COP21) commitments. Just recently, the European environment ministers agreed on a 35 % car emission cut of CO<sub>2</sub> by 2030 from recorded levels in 2020 [3]. Here, further trends are of particular interest. First, biofuels as high-density energy storage media for use in conventional combustion engines offer a significant reduction of greenhouse emissions using the current fossil fuels infrastructure. Second, innovative ignition systems to achieve ultra-lean combustion in spark ignited (SI) engines will result in better fuel economy and reduced NO<sub>x</sub> emissions.

Advanced biofuels use as feedstock non-food biomass and are of increasing interest concerning the replacement of fossil energy carriers for use in conventional combustion engines as they offer a significant reduction of greenhouse emissions using the current fossil fuels infrastructure. Different types of biofuels exist including oxygen-containing and nitrogenated species [4]. Energy stored in the fuel is converted to kinetic energy in the combustion process. Therefore, the combustion chemistry of advanced biofuels is of particular interest and a detailed knowledge of the combustion process can be used to improve the efficiency of SI engines. The knock behavior of advanced biofuels for example can be optimized with proper chemical synthesis i.e. future fuels can be designed for future cars to increase engine efficiency and reduce the emission [5]. Hence, it is of crucial importance to understand the ignition of future fuels in detail. In SI engines the use of spark plugs producing thermal plasmas has a long history [6]. However, a larger ignition volume can be obtained using specific non-thermal plasmas, which facilitates combustion in high exhaust gas recirculation engines or under ultra-lean combustion conditions. Here, in conjunction with an appropriate electrode design, a transient non-thermal plasma can take advantage of specific non-equilibrium chemistry to boost a more reliable ignition [7].

For the evaluation of the combustion of advanced biofuels and the efficiency of volumetric ignition systems it is necessary to understand the ignition process in detail. In this work, a combined experimental-numerical approach provides insight to the related physicochemical processes during the ignition by thermal and non-thermal plasmas to evaluate two different mechanisms by which an electrical discharge can affect the ignition of a combustible/air mixture. Typically, there are two necessary conditions for a successful ignition, namely the actual ignition event (short enough time for the formation of the radical pool) and the survival of the initially formed flame kernel (which is governed by the interaction of chemical kinetics and transport). The temporal development of the hot gas kernel and the subsequent flame propagation after ignition were

examined using a Schlieren method and laser induced fluorescence (LIF) of OH radicals. The ignition energy was varied to examine the interaction of convection, molecular transport and chemical reactions.

In case of non-equilibrium plasma, the dissociation and excitation of molecules by electron impact reactions can produce a significant number of active radicals and, therefore, can promote the ignition and initiate a chain reaction already at relatively low temperatures [8, 9]. High voltage alternating currents result in the formation and propagation of cathode-directed repetitive streamer discharges with a duration of several nanoseconds. The influence of mixture composition, applied voltage and number of streamer discharges on the ignition process and ignition volume was examined using chemiluminescence and OH-LIF. The experimental results are compared with numerical simulations in which the electron impact reactions are considered properly. Chemical pathway analysis shows more robust ignition and faster flame development in case of the repetitive streamer discharges compared to the capacitance sparks. This demonstrates the potential of non-thermal plasmas for volumetric ignition in SI engines.

## 2 Numerical simulation

Concerning the ignition by capacitance sparks the electrical discharge was modeled with a cylindrical shape by adding a source term to energy conservation equation [10]. The parameters describing the source term are set according to the experimental results [11]. The one-dimensional simulations were carried out using the program INSFLA for unsteady flames in laminar flow [12]. It does not consider the discharge in detail but is capable of solving the gas-dynamic equations and comprises a detailed transport model and detailed chemical kinetics. The conservation equations for mass, momentum, energy and species mass are solved using the method of lines. This results in a time-integration for the differential-algebraic equations which are obtained by spatial discretization using finite differences. The propane mechanism consists of 53 species and 592 elementary reactions [13].

For the numerical simulation of the ignition of H<sub>2</sub>/air mixtures by non-thermal plasmas using INSFLA also a cylindrical configuration of the streamer is assumed. The ignition source in [12] is represented using a source term in the energy conservation equation. For non-thermal plasmas an additional energy source term resulting from the non-equilibrium plasma has to be regarded [14]. The energy deposition as a result of inelastic collisions leading to excitation and dissociation of gas molecules takes place due to an accompanying change in enthalpy exciting or dissociating molecules due to electron impact reactions. The additional source term, therefore, takes into account this additional energy coupling into the system during the time a reduced electric field is accounted for in the calculation [15]. The reaction mechanism incorporates the plasma chemistry of a high-current discharge in hydrogen/air mixtures [16] and a kinetic scheme of the non-equilibrium discharge in nitrogen/oxygen mixtures [17] resulting in a mechanism consisting of 29 species and 182 elementary reactions [18, 19]. The rate coefficients of the electron impact reactions are determined by solving the electron Boltzmann equation in the classical two-term approximation for reduced electric fields between 1 Td and 1000 Td using the BOLSIG+ software and database [20, 21].

For a numerical examination of the ignition by non-thermal plasma a conventional electric spark ignition was used as a basis for comparison. In order to check the influence of the chemical mechanism we calculated ignition delay times. In Figure 1 calculated

ignition delay times of a stoichiometric  $H_2$ /air mixture as a function of temperature using three different reaction mechanisms are shown. The mechanism of Bowman [18] shows good agreement with the well-known mechanisms of Maas [12] and Ó Conaire [22]. Therefore, we use the mechanism of Bowman et al. [18], which accounts for electron impact reactions for the computation of both ignition scenarios (streamer discharge and conventional spark ignition).

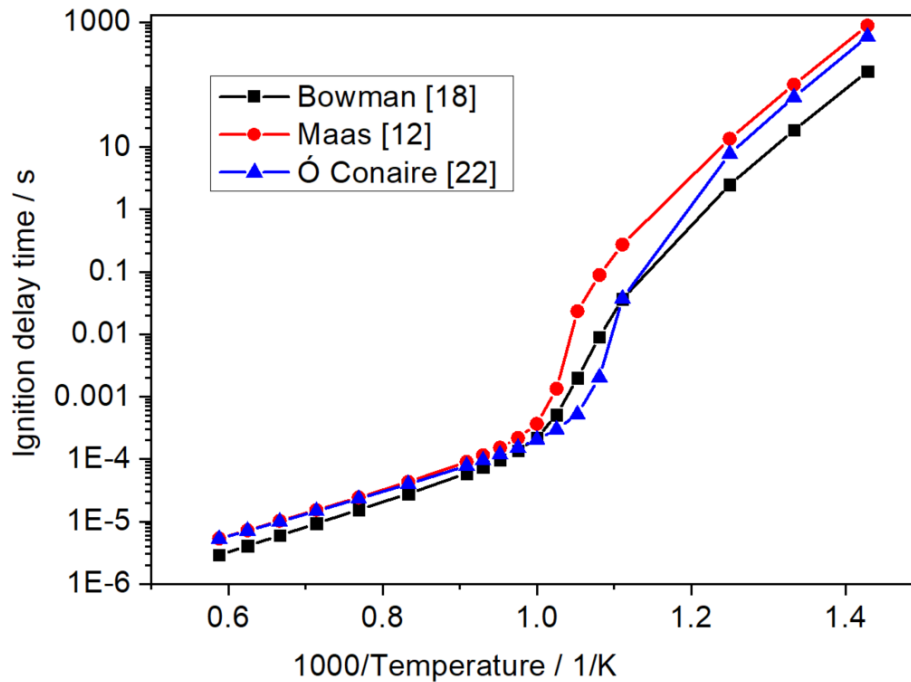


Figure 1: Ignition delay times of stoichiometric  $H_2$ /air mixture at 1 bar, calculated with different reaction mechanisms

### 3 Results

#### 3.1 Ignition by capacitive sparks

In a capacitive discharge, a high voltage  $U$  is applied to a capacitor and the stray capacitances of the electrical circuit,  $C$ . When this voltage exceeds the breakdown voltage for a sufficiently long time, the energy stored in the system,  $E = 1/2 CU^2$ , is released within a short time interval on the order of  $1 \mu s$ . A plasma channel forms between the electrodes of the ignition system due to the Townsend or the streamer mechanism [23]. This channel rapidly expands radially, and its electric resistance decreases, allowing strong currents to flow across the formerly non-conductive gas gap. Eckhoff [24] gave a comprehensive overview of energy balance of the processes following the electrical discharge which may lead to the ignition of a burnable mixture. In the following, we illustrate the most important sub-processes that govern the ignition by capacitive discharges. While a repeatable and secure ignition in an engine usually calls for high discharge energy, the consideration of much smaller discharge energies is useful to gain a detailed understanding of the ignition process. Also, some processes may be covered by very high discharge energies but may still deserve consideration e.g. in a numerical model for the prediction of the ignition and flame propagation. Therefore, we illustrate the processes using the example of a 5.2 vol. % propane/air mixture with discharge energies of several hundred  $\mu J$ . The tungsten electrodes with rounded tips

have a diameter of 2.4 mm and the electrode distance is 1.7 mm. The energy is close to the minimum amount needed to ignite this mixture in an optimized setup [25].

### 3.1.1 Expansion of the hot gas channel and the pressure wave

The deposition of the discharge energy in a short amount of time in a small volume results in high gas temperatures and pressures. This leads to the rapid expansion of a hot gas channel. Also, a shock wave forms at the perimeter of the hot channel. The shock wave will separate from the channel and travel outwards at supersonic speed, slightly heating the gas in the surrounding as it passes. Depending on the discharge energy, the shock wave decays rather quickly to a sound wave with velocity  $Ma = 1$ . In the following, the term pressure wave will be used as it includes both the shock and the sound wave.

Figure 2 shows the expansion of the hot gas channel and the pressure wave for propane. The data was obtained via schlieren measurements at different times after the discharge. From the single-shot images, the respective radii were extracted [11]. The data shows that the expansion of the gas channel occurs in distinct phases. Within the first microsecond following the discharge, the channel grows rapidly due to high temperature and pressure. A plasma induced pressure wave is distinguishable from the channel after  $0.5 \mu\text{s}$ . In this particular case, its speed is  $Ma = 1.4$  but quickly reduces to  $Ma = 1$  after around  $30 \mu\text{s}$ . After the detachment of the pressure wave, the hot channel expansion slows considerably. A second stage of expansion follows, starting after around  $10 \mu\text{s}$ , which is governed mainly by the flow field induced by the discharge and the geometry of the electrodes [26, 27]. This second expansion phase is orders of magnitude slower than the first one.

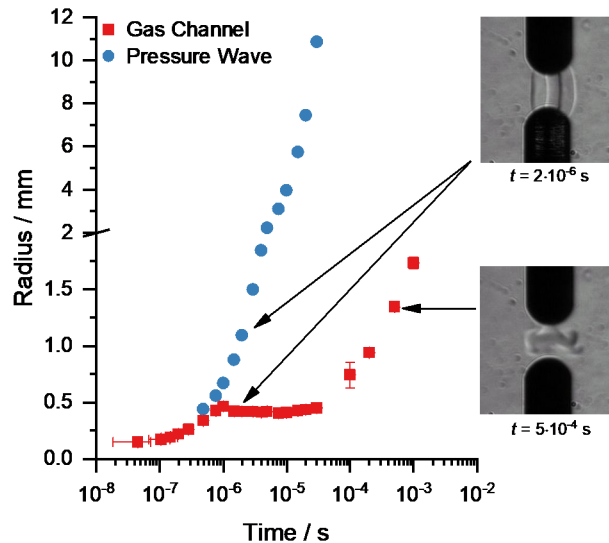


Figure 2: Temporal evolution of the hot gas channel and the pressure wave following a capacitive discharge in a 5.2 vol. % propane/air mixture. The discharge energy was  $240 \mu\text{J}$ . Each data point corresponds to the average of at least five experiments; the error bars indicate their standard deviation. The insets show a typical schlieren image  $2 \mu\text{s}$  and  $500 \mu\text{s}$  after the discharge. The hot gas channel and the pressure wave are clearly visible.

Numerical models allow the simulation of this expansion process. We introduced an efficiency factor in the source term of our model and simulated the expansion of the channel and the pressure wave for several efficiencies. The best agreement between

the results from this numerical model with the experimental data allowed us to determine the efficiency of the discharge. For a 249  $\mu\text{J}$  discharge in air we found that the efficiency was approximately 40 % [28].

### 3.1.2 Early phase of flame propagation

The temperature increase due to the capacitive discharge starts chemical reactions in the burnable mixture. When the energy input is finished (50 to 100 ns in the case considered here), the energy balance between heat released by the combustion reactions and heat transfer to the electrodes and the surrounding cold gas is the deciding factor as to whether an ignition will occur or not. If the discharge energy is sufficiently large, loss processes are irrelevant and need not be modelled. However, a detailed analysis of these processes may aid in designing improved ignition systems. Their proper investigation demands that the discharge energy is at a level where ignition is equally or even less likely than non-ignition.

We investigated the early phase of flame propagation using high-speed schlieren videography [29] and single-shot laser-induced fluorescence of the OH radical (OH-LIF) [30]. Typical results for the ignition phase in the propane/air mixture are shown in Figure 3. Experiments for two energies are compared, a low energy ( $E = 480 \mu\text{J}$ ) where the ignition probability is only 1 % and a higher energy ( $E = 960 \mu\text{J}$ ) with an ignition probability of 75 %. The ignition probabilities were calculated using a logistic regression model [31]. For each energy, the top row shows four frames extracted from a high speed schlieren video while in the bottom row single-shot planar OH-LIF images are shown. In the examples shown, the lower energy does not lead to an ignition while the higher energy discharge successfully ignites the mixture. The schlieren images indicate the region where the temperature is significantly higher than in the unperturbed surrounding. It needs to be kept in mind that this technique integrates the changes of the refractive index over the depth of the interrogation volume. Thus, the images do not show the flame directly but allow for an interpretation of the fluid dynamics that influence the ignition process. The OH-LIF images, on the other hand, present a 2D cut through the center of the flame and, as OH is an intermediate species of the combustion reaction, indicate the regions where combustion reactions are taking place.

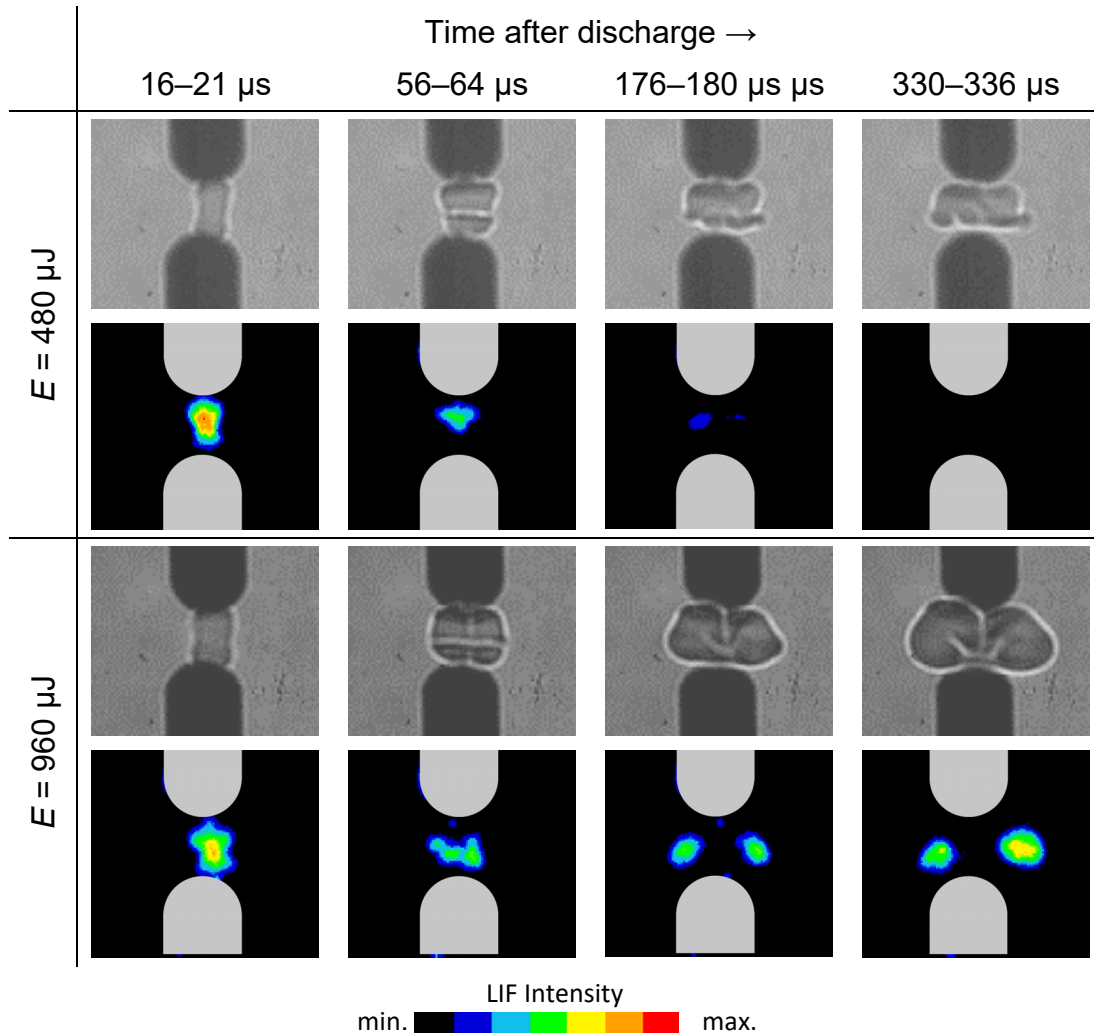


*Figure 3: Evolution of the early flame kernel in a 5.2 vol. % propane/air mixture after a capacitive discharge at two energies. For each energy, single frames from a high-speed schlieren video and single-shot OH-LIF images are given in the top and bottom row, respectively. In the LIF images, the electrodes were added as grey shapes for better orientation.*

The schlieren images reveal that starting from a near-cylindrical channel in the first frame, a complex three-dimensional shape of the flame kernel develops within 50  $\mu\text{s}$ . As was seen in the previous section, the growth of the kernel due to the gas-dynamic expansion is slow for times greater than 1  $\mu\text{s}$  after the discharge. The further expansion is a superposition of the flow field induced by the discharge and the combustion. It is faster when the energy is increased. The last two schlieren frames of the higher-energy case show how a non-spherical flame develops and expands outwards. In the lower-energy case, no ignition occurs and the hot kernel cools down. It is no longer detectable after some milliseconds (not shown here).

The OH-LIF images also illustrate the complex change of shape of the reaction zone. Between frames two and three, it splits into two distinct regions, indicating a toroidal flame. At both discharge energies, the intensity and therefore the OH concentration decrease significantly up to about 180  $\mu\text{s}$ . However, in the high-energy case, the temperature in the kernel is still high enough to allow for a self-sustained flame propagation, seen in the last frame. In the lower-energy case, the cooling due to the electrodes

and the surrounding cold gas draws more energy from the reaction zone than what is produced by the chemical reaction. Therefore, the OH signal decays to zero and the reaction stops.

In Figure 4 the calculated temporal evolution of maximum temperature and maximum OH mole fraction is displayed for the same two ignition energies. In the higher energy case, there is a large temperature rise up to 6300 K due to the energy deposition by the source term. This goes along with a significant formation of OH radicals. The temperature and formation of OH is high enough to form a self-sustaining flame. For the lower energy level, the temperature rise up to 50 ns is much lower, it does not exceed 2500 K. A significant formation of OH starts only after the energy deposit has ended due to beginning combustion reactions. However, much less OH is formed compared to the higher energy level and cooling in addition prevents an ignition of the mixture.

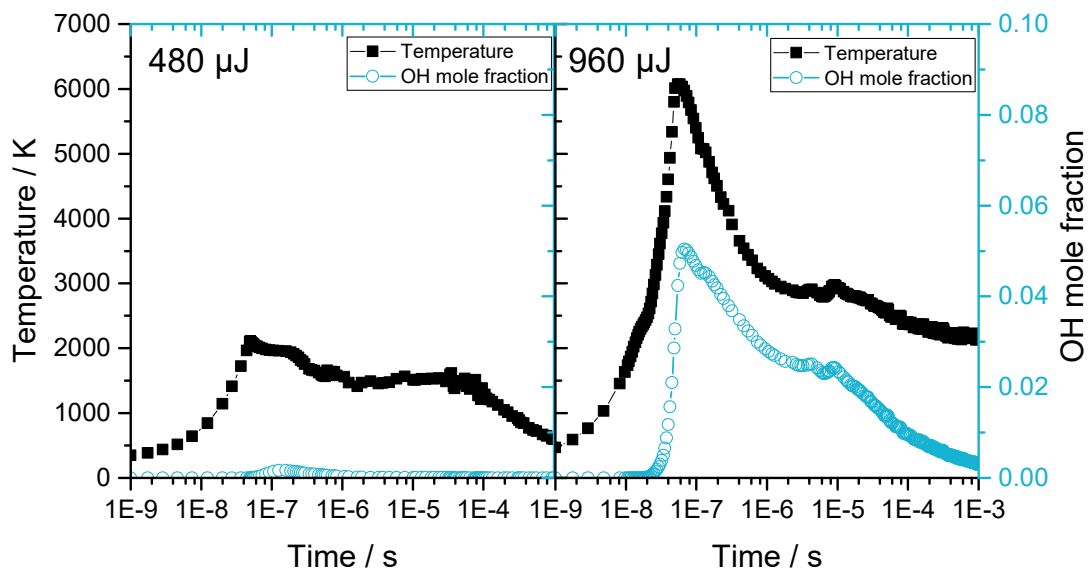


*Figure 4: The temporal profiles of maximal temperature and OH mole fraction for two different energy levels. The left column shows results of a non-ignition (source radius 200  $\mu\text{m}$ ) and the right column calculation of ignition (source radius 150  $\mu\text{m}$ ).*

Figure 5 compares experimental and numerical results regarding the radial profiles of the OH radical. In the left column, the normalized LIF intensity from the experiment is shown on the vertical axis. The different results for repeated experiments illustrate the stochastic variability of the ignition process. In the right column, the OH mole fraction extracted from numerical simulations is plotted. The top row shows an early time instant corresponding to the first time step in Figure 3. A comparison of the experimental results at the two energies shows that the flame kernel is larger in diameter when the energy is higher. Also, the intensity of the signal is stronger. These trends are well captured in the numerical simulation. The approximately Gaussian shape of the LIF profiles at this early time step is reproduced. In the bottom row, a time step during the evolution of the flame kernel is shown, corresponding to the third time step in Figure 3. Here, the differences between the two ignition energies are obvious. At the higher energy, the center of the flame kernel has travelled 1 mm from the electrode axis and the measured LIF intensity is still strong. However, for the lower-energy discharge the flame kernel has travelled a significantly shorter distance away from the electrodes and the LIF intensity is reduced significantly. In the simulation, the higher ignition energy

correctly leads to a larger flame diameter at this point. While the flame front position is given correctly by the numerical simulation, there is a discrepancy between the radial OH profiles near the center of the former plasma channel. Mainly due to cooling by the electrodes the OH radicals vanish in the experiment. This effect was not considered in the numerical simulations. While they have no influence on the subsequent flame propagation, they may disturb the ignition of combustible mixtures with longer ignition delay time and have to be considered then using 2D models e.g. as in [26].

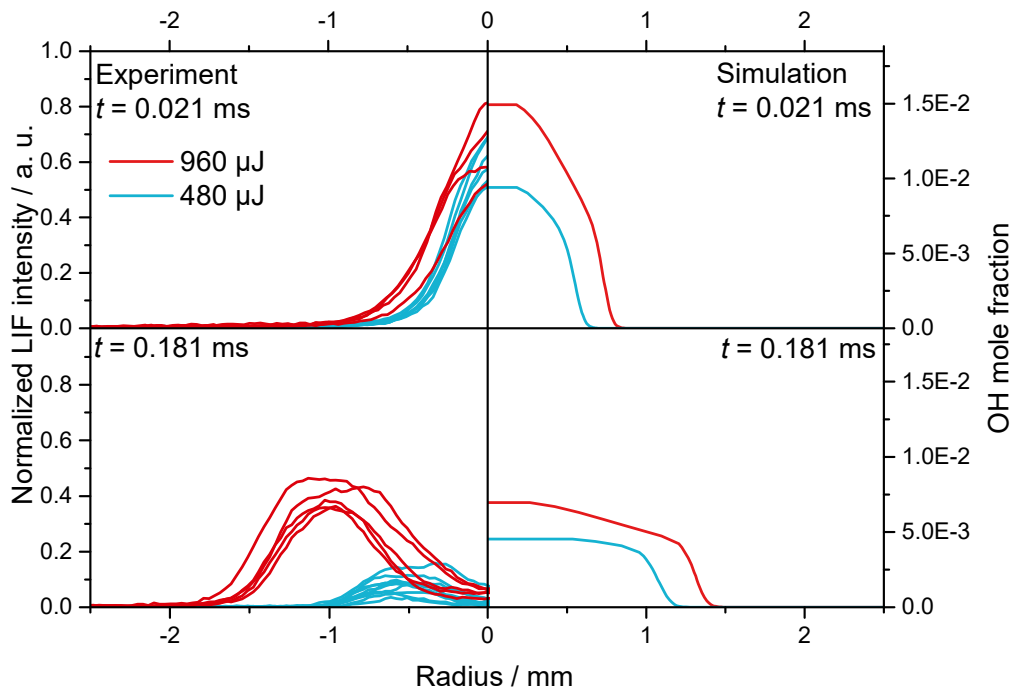


*Figure 5: Radial profiles of the normalized LIF intensity measured in the experiment (left column) and of the OH mole fraction from the numerical simulation (right column). Two time steps are shown (top and bottom row). For each time step, two energies are depicted. Several realizations of the experiment are shown to illustrate the stochastic variability of the ignition process*

As these results show, complex interactions between chemistry, fluid dynamics and transport processes such as heat transfer overlap each other even in this simple and initially quiescent setup. The conditions in an engine add further difficulty to the problem: inhomogeneous, multi-phase mixtures including exhaust gas from the previous stroke, turbulent flow fields, more complicated geometries and temperature fields need to be accounted for. Nevertheless, the aforementioned aspects should not be neglected. In particular, detailed chemical kinetics and transport processes are needed to properly describe ignition processes.

### 3.2 Ignition by streamer discharges

A high voltage pulse leads to a streamer discharge and if the pulse is too short in time to result in a spark breakdown the energy deposition takes place mainly in the streamer head [32]. Currents between 0.1 and 1 mA can be measured in the voltage range of 10 to 100 kV and only negligible heating occurs during one single streamer discharge. Repetitive streamer discharges, however, can be used to achieve a volumetric ignition

of combustible/air mixtures. Using an alternating voltage in a rod/plane configuration in which the plane is grounded, an intensive streamer discharge occurs for approximately 100 ns as can be seen in Figure 6 if positive voltage is supplied to the rod [15]. While at 9 kV only one streamer channel is visible after 100 voltage cycles, several plasma channels are visible using 11 kV. Due to the long exposure time of 140  $\mu$ s the light emission of several hundred streamer discharges is shown in Figure 6.

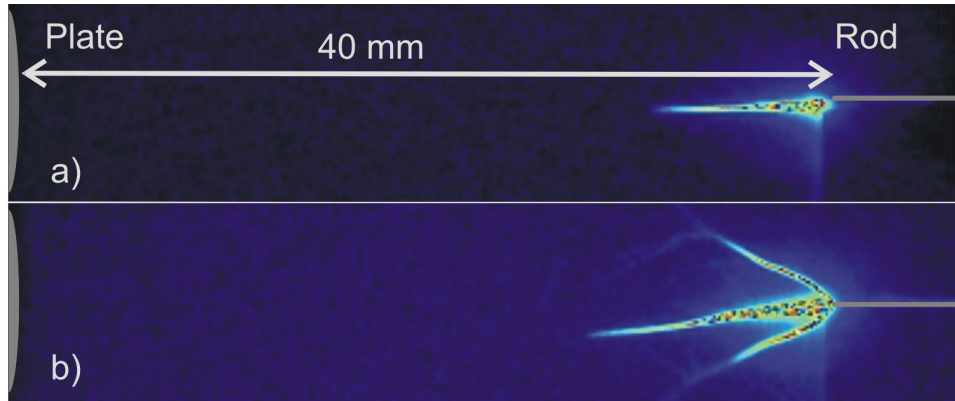


Figure 6: Streamer discharges after 100 voltage cycles at 740 kHz, exposure time 140  $\mu$ s a)  $\hat{U} = 9$  kV, b)  $\hat{U} = 11$  kV

The physical and chemical processes of plasma-assisted ignition and plasma-assisted combustion have been in the focus of research for several years now [8, 9, 33]. It is well known that using non-thermal plasmas as an ignition source the overall energy necessary for ignition is approximately the same or less than that required for conventional spark ignition [28, 34]. The mean electron energy here is determined by a reduced electric field  $E/N$ , where  $E$  is the electric field and  $N$  is the gas density [8]. A comparison of the temporal development considering either a reduced electrical field of 0 Td (spark ignition) or 300 Td (non-thermal plasma) reveals that a lower temperature is necessary for ignition (Figure 7a). For both reduced electrical fields the minimum amount of energy necessary for ignition was used, i.e. using lower energies would result in non-ignition in both cases. Even though additional energy deposition occurs due to electron impact reaction using non-thermal plasmas, they are more efficient concerning the energy necessary for ignition [15]. Due to electron impact reactions the dissociation of  $O_2$  and  $H_2$  results in a great number of radicals even at low temperatures. As shown in Figure 7b directly after the first streamer discharges in the numerical simulation a strong increase of O, H and OH radicals occurs. The formation of these radicals via Arrhenius-type elementary reactions in case of the thermal plasma takes much longer to produce a similar number of radicals.

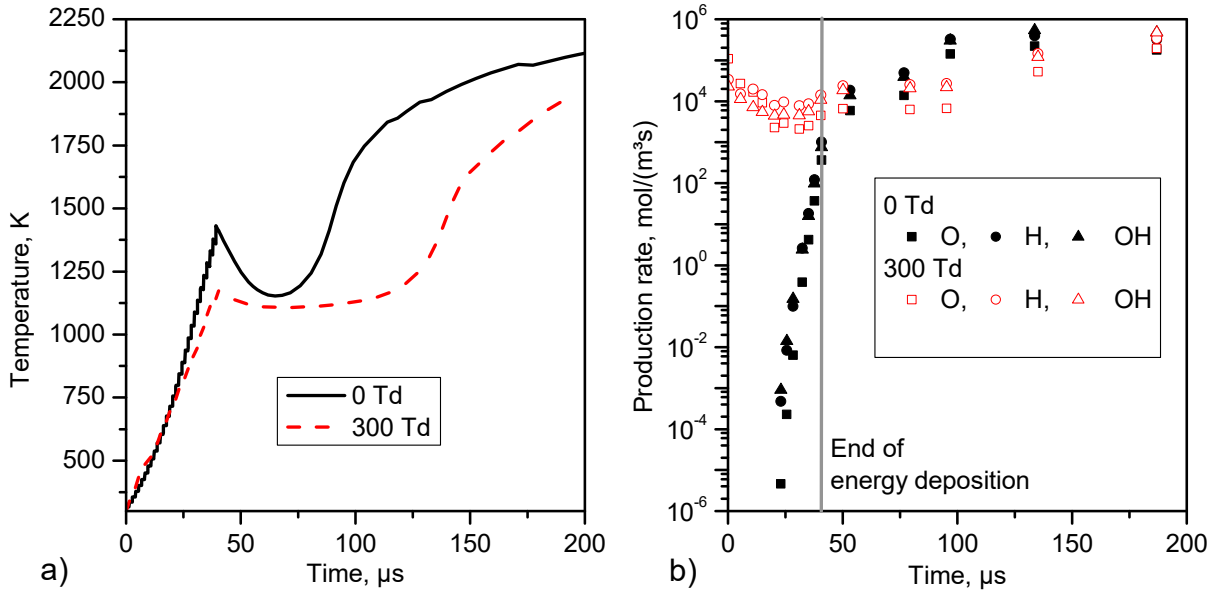


Figure 7: Comparison of the ignition of a 25 vol.%  $\text{H}_2$  in air mixture by a thermal plasma (0 Td) and a non-equilibrium plasma (300 Td); a) maximum temperature in the computational domain, b) production rate of O, H and OH (reprint from [35]).

As was shown in Figure 6 a distance of 40 mm between rod and plate was used to examine the ignition of  $\text{H}_2/\text{air}$  mixtures by streamer discharges experimentally. A sequence of OH images using a peak voltage of 14 kV and 100 voltage cycles corresponding to an energy deposition time of 140  $\mu\text{s}$  is shown in Figure 8. From numerical simulations it is known that there is a temperature gradient along the plasma channel [36]. Starting with a maximum temperature near the tip of the rod the temperature inside the plasma channel decreases towards the end of the channel. As is visible in Figure 8 the ignition starts around 110  $\mu\text{s}$  near the tip of the rod. However, after 160  $\mu\text{s}$  the whole plasma channel has led to ignition and afterwards the subsequent flame propagation perpendicular to the plasma channel can be seen. A further increase of energy would shorten the ignition delay time. Additionally, using higher energies results in additional plasma channels which would enlarge the volume of ignition.

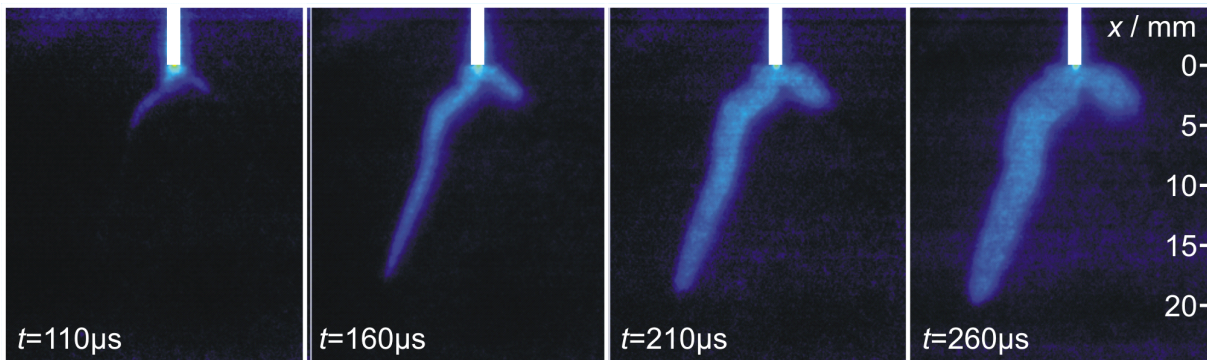


Figure 8: Sequence of OH-LIF images of an ignition along the whole streamer channel (25 vol.-%  $\text{H}_2$ ,  $\hat{U} = 14$  kV, 100 voltage cycles)

## 4 Conclusions

Alternative fuels like advanced biofuels and more efficient combustion engines can promote further reduction of CO<sub>2</sub> and pollutant emissions in the road transportation sector. For both topics a detailed understanding of the ignition process will help to support these developments using numerical simulations. Fundamental work on the probability of ignition and the dominating factors considering spark ignition of quiescent mixtures helps to improve numerical tools like INSFLA used in this work. The comparison of experimental and numerical results considering spark ignitions using detailed chemical kinetics demonstrates qualitatively good agreement despite the restriction to a one-dimensional (cylindrical) model. This offers the opportunity to examine the ignition of advanced biofuels in depth which will support the development of detailed reaction mechanisms.

The ignition by non-thermal plasmas like repetitive streamer discharges of up to 100 ns as examined in this work have shown significant advantages compared to the ignition by conventional spark ignition. The proper use of non-thermals plasmas may help to reduce ignition delay time compared to conventional spark ignition and enables volumetric ignition which would support the development of high exhaust gas recirculation engines or ultra-lean combustion engines. A deeper knowledge of the non-thermal plasma processes like electron impact reactions is necessary to understand the ignition by non-thermal plasmas more in detail. Again, numerical tools like INSFLA can be used to examine the fundamental physical and chemical processes and will, therefore, support the development of modern engine concepts.

## References

- [1] Umweltbundesamt, Kohlendioxid-Emissionen, <http://www.umweltbundesamt.de/daten/klimawandel/treibhausgas-emissionen-in-deutschland/kohlendi-oxid-emissionen>. Accessed 11 Oct 2018.
- [2] Directive 2009/28/EC, Directive 2009/28/EC of the European Parliament and of the Council of 23 April 2009 on the promotion of the use of energy from renewable sources and amending and subsequently repealing Directives 2001/77/EC and 2003/30/EC.
- [3] The European council, CO<sub>2</sub> emission standards for cars and vans: Council agrees its position, <https://www.consilium.europa.eu/en/press/press-releases/2018/10/10/co2-emission-standards-for-cars-and-vans-council-agrees-its-position/>. Accessed 11 Oct 2018.
- [4] K. Kohse-Höinghaus, P. Oßwald, Terrill A. Cool and Tina Kasper, N. Hansen, F. Qi, C. K. Westbrook, P. R. Westmoreland, *Angew. Chem., Int. Ed.* 2010, 49, 3572 – 3597. DOI: 10.1002/ange.200905335.
- [5] W. Leitner, J. Klankermayer, S. Pischinger, H. Pitsch, K. Kohse-Höinghaus, *Angew. Chem., Int. Ed.* 2017, 56 (20), 5412 – 5452. DOI: 10.1002/anie.201607257.
- [6] R.R. Maly, *Symp. (Int.) Combust.* 1994, 25 (1), 111 – 124. DOI: 10.1016/S0082-0784(06)80635-1.
- [7] T. Shiraishi, A. Kakuho, T. Urushihara, C. Cathey, T. Tang, M. Gundersen, *SAE Int. J. Engines* 2009, 1 (1), 399 – 408. DOI: 10.4271/2008-01-0466.
- [8] S. Starikovskaia, *J. Phys. D: Appl. Phys.* 2006, 39, R265-R299. DOI: 10.1088/0022-3727/39/16/R01.

- [9] S. M. Starikovskaia, *J. Phys. D: Appl. Phys.* 2014, 47 (35), 353001. DOI: 10.1088/0022-3727/47/35/353001.
- [10] A. Dreizler, S. Lindenmaier, U. Maas, J. Hult, M. Aldén, C. F. Kaminski, *Appl. Phys. B* 2000, 70, 287 – 294. DOI: 10.1007/s003400050047.
- [11] S. Essmann, *Plasma Phys. Technol.* 2016, 3 (3), 116 – 121.
- [12] U. Maas, J. Warnatz, *Combust. Flame* 1988, 74, 53 – 69. DOI: 10.1016/0010-2180(88)90086-7.
- [13] C. Chevalier, Entwicklung eines detaillierten Reaktionsmechanismus zur Modellierung der Verbrennungsprozesse von Kohlenwasserstoffen bei Hoch- und Niedertemperaturbedingungen, Dissertation, University of Stuttgart 1993
- [14] T. Langer, D. Markus, U. Maas, in 42<sup>nd</sup> AIAA Plasmadynamics and Lasers Conference 2011. DOI: 10.2514/6.2011-3450.
- [15] T. Langer, Zündung von Wasserstoff/Luft-Gemischen durch repetierende Teilentladungen, Dissertation, Karlsruhe Institute of Technology 2013.
- [16] N. A. Popov, *Plasma Phys. Rep.* 2008, 34, 376 – 391. DOI: 10.1134/S1063780X08050048.
- [17] I. A. Kossyi, A. Y. Kostinsky, A. A. Matveyev, V. P. Silakov, *Plasma Sources Sci. Technol* 1992, 1, 207 – 220. DOI: 10.1088/0963-0252/1/3/011.
- [18] S. Bowman, I. Choi, K. Takashima, I. V. Adamovich, W. R. Lempert, in 48<sup>th</sup> AIAA Aerospace Sciences Meeting 2010.
- [19] M. Uddi, N. Jiang, I. V. Adamovich, W. R. Lempert, *J. Phys. D: Appl. Phys.* 2009, 42, 75205. DOI: 10.1088/0022-3727/42/7/075205.
- [20] G J M Hagelaar, L. C. Pitchford, *Plasma Sources Sci. Technol* 2005, 14 (4), 722 – 733.
- [21] BOLSIG+, <https://www.bolsig.laplace.univ-tlse.fr/>. Accessed 11 Oct 2018.
- [22] M. Conaire, H. Curran, J. Simmie, W. Pitz, C. Westbrook, *International Journal of Chemical Kinetics* 2004, 36, 603 – 622. DOI: 10.1002/kin.20036.
- [23] A. Küchler, *High Voltage Engineering: Fundamentals - Technology - Applications*, VDI-Buch, Springer Berlin Heidelberg; Imprint; Springer Vieweg, Berlin, Heidelberg 2018.
- [24] R. K. Eckhoff, W. Olsen, *J. Electrostat.* 2010, 68 (1), 73 – 78. DOI: 10.1016/j.elstat.2009.11.001.
- [25] E27 Committee, Test Method for Minimum Ignition Energy and Quenching Distance in Gaseous Mixtures, ASTM International, West Conshohocken, PA.
- [26] S. P. M. Bane, J. L. Ziegler, J. E. Shepherd, *Combust. Flame* 2014 (0). DOI: 10.1016/j.combustflame.2014.07.017.
- [27] M. Thiele, J. Warnatz, U. Maas, *Combust. Theor. Model.* 2000, 4 (4), 413 – 434. DOI: 10.1088/1364-7830/4/4/303.
- [28] D. Markus, S. Essmann, J.-R. Kummer, R. Shekhar, C. Uber, U. Gerlach, U. Maas, *Z. Phys. Chem.* 2017, 231 (10), 1655 – 1682. DOI: 10.1515/zpch-2016-0903.
- [29] S. Essman, D. Markus, U. Maas, in 26<sup>th</sup> International Colloquium on the Dynamics of Explosion and Reactive Systems. Boston 2017.
- [30] S. Essmann, J. R. Kummer, D. Markus, U. Maas, in Proceedings of the twelfth International Symposium of Hazards, Prevention, and Mitigation of Industrial Explosions. Kansas City 2018.
- [31] A. Wähner, G. Gramse, T. Langer, M. Beyer, *J. Loss Prevent. Proc.* 2013, 26 (6), 1655 – 1660. DOI: 10.1016/j.jlp.2013.06.002.
- [32] T. Langer, D. Markus, F. Lienesch, U. Maas, *Combust. Sci. Technol.* 2010, 182, 1718 – 1734. DOI: 10.1080/00102202.2010.497374.

- [33] A. Y. Starikovskii, N. B. Anikin, I. N. Kosarev, E. I. Mintoussov, S. M. Starikovskaia, V. P. Zhukov, *Pure Appl. Chem* **2006**, 78, 1265 – 1298. DOI: 10.1351/pac200678061265.
- [34] D. Singleton, S. J. Pendleton, M. A. Gundersen, *J. Phys. D: Appl. Phys.* **2011**, 44 (2), 22001. DOI: 10.1088/0022-3727/44/2/022001.
- [35] D. Markus, T. Langer, U. Maas, in: *44<sup>th</sup> AIAA Plasmadynamics and Lasers Conference*. San Diego **2013**. DOI: 10.2514/6.2013-3006.
- [36] D. Markus, T. Langer, U. Maas, in *24<sup>th</sup> International Colloquium on the dynamics of explosions and reactive systems*. Taipeh **2013**.